X-RAY FLUORESCENCE AND THE QUATERNARY SYSTEM $Ga_xIn_{1-x}As_ySb_{1-y}$

by

Denis Martel

Submitted in partial fulfillment of the
requirements for the degree of Master of Science

Department of Physics
Faculty of Science and Engineering
University of Ottawa
Ottawa, Ontario
July 1972

REMERCIEMENTS

J'aimerais exprimer ici toute ma gratitude et mes remerciements les plus sincères à M. J.C. Woolley pour les conseils et pour l'assistance soutenue qu'il m'a témoigné tout au cours de ces travaux, qui ont permis la réalisation de cette thèse. Serait-il vain d'ailleurs de témoigner mon égale reconnaissance à tous ceux qui ont contribué, directement ou indirectement, à ces recherches; pour n'en citer que quelques-uns: M. R. Fournier pour sa collaboration en programmation, le groupe de l'état solide, stimulant par sa présence et ses discussions, Mlle S. Kwan qui a prêté sa main à maints graphiques, le gouvernement de l'Ontario pour son aide financière...

D'autre part, j'aimerais dédier cette thèse à mes parents et à Geneviève, sans qui cette thèse ne serait pas.

ABSTRACT

In this work, radioisotope X-ray fluorescence with a Si(Li) detector is used to determine the composition of a quaternary alloy of Gallium, Arsenic, Indium and Antimony. The intensity ratios of the characteristic radiation peaks are computed for powdered standards, and "working curves" established as a function of composition to obtain a rapid quantitative determination, of the order of one or two per cent, by a comparison method. The phase diagram of this system is partially investigated together with the lattice constant variation with composition.

INTRODUCTION

A few years ago, the advent of high resolution X-ray detectors made possible resolution of less than 180 eV FWHM (Full Width at Half Maximum) for Iron K-alpha X-rays, even at high count rates. The simultaneous development of fast, large memory, multichannel analysers also contributed in making energy dispersive X-ray fluorescence spectroscopy (ED-XRF or XRF) one of the most valuable instruments available to the analyst[1,2,3]. This technique by which a specimen is irradiated by an X-ray source and emits characteristic fluorescent radiation is now common in geology, mineral engineering and in other fields where a non-destructive composition determination is required[4,5,6,7]. Many on-stream analyses, for example, require such a fast determination, which is accelerated by the use of small computers and advanced datahandling techniques; XRF then allows an immediate qualitative multi-element identification, and their subsequent quantitative determination.

Although radioisotope XRF is not comparable in accuracy and detection limits to the conventional techniques, i.e. microprobes and wavelength dispersive spectrometers, its superiority becomes obvious in the following cases:

1- When many elements are to be detected in a short time; because spectrometers are limited to a single

wavelength at a time.

2- Cost and working space are reduced with XRF; because radioisotopes eliminate the use of expensive and high power X-ray tubes, so that the volume occupied and the calibration operations are reduced.

3- Particle size effects and matrix effects are less emphasized, because radioisotopes are available at higher primary radiation energy than X-ray tubes to excite the K-shell radiation of the heavy elements.

These reasons made XRF the best analytical instrument available for the particular problem of determining the composition of a III-V semiconductor quaternary alloy, consisting of the elements Gallium, Arsenic, Indium and Antimony of atomic numbers 31,33, 49 and 51 respectively.

INSTRUMENTATION: X-RAY FLUORESCENCE

A- DETECTOR

Sensitivity and resolution are two characteristics of a good detector and consequently, of a good analysis. Thus parameters which contribute to performance are:

-Sensitive depth: All the energy must be deposited in the sensitive region in order that the output pulse height be proportional to the energy of the incident X-ray.

-Area: The area determines counting rate efficiencies and energy resolution.

-Small Signal Capacitance: For low total noise, it is necessary to minimize the detector capacitance by restricting the active area and/or optimizing the sensitive depth.

-Electric Field Intensity and Breakdown Voltage: The electric field strength required to insure complete charge collection must exceed some minimum value in order to optimize resolution and linearity response, but, for a given resistivity material, the breakdown voltage of the diode establishes an upper limit on the sensitive depth and on the electric field required.

-Reverse Leakage Current: A large diode leakage current results in detector noise and excessive voltage drop across the bias supply resistor.

These requirements almost completely determine the final energy resolution and detector-preamplifier noise, customarily specified in terms of the FWHM (full width at half maximum) broadening of a monoenergetic peak. Dead layer thickness, pulse rise time, thickness uniformity, crystal orientation are other variables which contribute to final performance, but most detectors are now commercially avai-

lable at very high standards.

Our detector, including the preamplifier and liquid nitrogen assembly (cold finger dipped in a liquid nitrogen dewar), was bought from Nuclear Diodes Inc., Illinois. The Lithium-drifted Silicon detector, Si(Li), used had a circular cylindrical configuration with an active area of 30 mm^2 and a 3 mm depletion depth, located 4 mm below a .003 inch thick beryllium window (FIG 1-C). This window needs to be thick enough to sustain the pressure due to the vacuum inside the detector housing, but thin enough to minimize the absorption of incident X-ray by the window material. This is why a low atomic number (Z=4) element is used: Beryllium.

System resolution was guaranteed to be 179 eV FWHM, for a 5.9 KeV Manganese Fe^{55} source, when a negative bias of 250 volts is applied to the detector.

B- SOURCE AND SAMPLE HOLDER

The wide variety of possible sources available for radioisotope XRF requires a careful choice of exciting energy, for a particular analysis. Source requirements are low cost, availability with high specific activity, long half-life and high sensitivity, relative to the excitation of the elements in the unknown. Iodine-125, a relatively short-lived isotopic source was our solution. TABLE 1-A and 1-C give data on the emission energies of the ^{125}I source, and on the emission energies of the elements to be determined. Although the K_α X-ray of Te fall below the absorption edges of Indium and Antimony, these are efficiently excited by the 35.5

KeV and the K_β radiations of the source. But detection limits on Indium and Antimony of a few parts per million are still obtained, the reason for this lies in the fact that analytical sensitivity can be achieved by using a source-target which has its exciting energies just above the absorption edges of the elements to be determined. Although Gallium and Arsenic do not enjoy a similar privilege, they are still well above the accuracy limit required for our experiments (cf. below).

Moreover, this source was readily available to us from AECL (Atomic Energy of Canada Ltd., Commercial Products Division) at a high intensity, i.e. more than 100 milliCuries. A Tin and Brass collimator was used to hold and focus the source on to the sample.

A source holder was designed to hold the source-collimator assembly and to provide a large useful working-space above the detector. The geometrical arrangement of source, sample and detector is such as to minimize the path-length of the incident and characteristic radiations, thus reducing absorption and scattering effects and maintaining a high count rate (FIG. 1-A). A vacuum chamber also was built but will not be described here since it was not used in the present experiments.

All standards and unknowns to be analysed were powders contained in a small sample holder, illustrated in FIG. 2. The polyethelene wrap, when stretched, makes a very thin ($<50\mu$) surface which does not absorb ($<.01\%$ absorption) the characteristic radiation of the samples.

C- ELECTRONICS

The detector bias was provided by a stable bias-voltage power supply (Nuclear Diode model ND-402). A field effect transistor, mounted with the detector in the cryostat, served as the first stage of a charge-sensitive preamplifier. The output of this preamplifier was followed by a DC coupled linear amplifier, consisting of 5 stages (three of which are integrated circuit operational amplifiers using active integration in their feedback loops), one RC differentiator, a baseline restorer and interchangeable time constants (1 to 6 μsec).

The multichannel analyser was a Kicksort Nuclear Diode model 705/706. Useful features of this 1024 channel pulse height analyser are a fast analog to digital converter with a 60 MHz conversion speed, an automatic timer with a dead time meter, add or subtract facility, a live 5 inch CRT display, a memory size selector, digital offset, etc...

The output was conveniently recorded on paper tape and printout via a teletype interface. The analyser could be programmed to accumulate for a given time then to print the data automatically. Unfortunately, all paper tapes had to be converted into IBM cards, by a PDP computer used as a terminal of the main computer. This cumbersome procedure was required in order to have a large computer, University of Ottawa's IBM 360/65, manipulate and fit the spectra.

The electronic circuitry is shown diagrammatically in FIG 3.

D- SPECTRA ANALYSIS

In all spectra, the same four elements are seen at the same location, or channel number, as determined by calibration of the amplifier gain. A typical spectrum is shown in FIG. 4-A and 4-B, in a semilogarithmic scale. Here, the Indium and Antimony peaks do not follow a simple Gauss distribution law, but are the summation of two Gaussians, i.e. the overlapped K_{α_1} and K_{α_2} radiations in the Indium and Antimony K_α peaks. Of course all peaks are combinations of alpha and beta components[11], although it is only for heavy elements, with high caracteristic energies, that the doublet separation becomes appreciable. The Gallium K_α radiation, for example, comsists of two peaks 0.027 KeV apart, which obviously is far beyond the enrgy resolution of the detector; whereas in Antimony, although the K_{α_1} and K_{α_2} peaks are not resolved as such, they still can be detected as two contributions to the overall K_α peak. Difference in energies in this case is of 248 eV (Note that the detector would have a resolution of approximately 340 eV FWHM in that region of the spectrum) as can be seen from TABLE 1-C listing the most important characteristic X-ray emission energies of Ga, As, In and Sb. It must be remembered that the K_{α_2} and K_{β_2} are fractions of the intensities of their respective K_{α_1} and K_{β_1}.

In order to fit the peaks, a computer program from Nuclear Physics was modified. Each spectrum was divided into three

regions; the first region enclosed only the Gallium K_α peak. The maximum and FWHM of this peak were computed as for a Gaussian distribution, and the background, approximated by a straight line, was obtained by interpolating the points on both sides of the peak. FIG. 1-A demonstrates how the Ga resolution remains unchanged even at high count rates. In fact, this graph gives the standard deviation on the Gallium peak resolution taking into account errors due to count rates, fitting by the program and statistical errors. Resolution is then seen to be 208 eV with a standard deviation of 2.9 eV, giving an error of 1.4%.

The second region encloses the K_β peak of Arsenic only. Although it is generally a low intensity peak, the K_β being a fraction of the K_α radiation, the error associated with this peak is still smaller than the error which would have been produced from the separation, fitting and integration of the K_α of Arsenic, which is overlapping with the K_β of Gallium. Again, a simple Gaussian associated with a linear background is a good approximation. Four peaks are now grouped in the third region: the K_α of Indium, which becomes the summation of two Gaussians, as discussed above; the Compton backscattered peak, enclosed in a very large Gaussian; the Antimony K_α peak, treated as the Indium K_α; and the K_β's of Indium, fitted as a single Gaussian. All peaks had to be analysed simultaneously due to a partial overlapping.

Various count rates were tried with no apparent deterioration

of resolution (FIG. 1-A). For a given time, high count rates were efficient in decreasing the statistical error for each channel, the standard deviation known to be $\sqrt{N}$ for a count of N. Accumulation times of twenty to forty minutes then provides peaks with counts as high as 100,000 with a relative error of 0.31%, but peaks for low concentration elements were sometimes of the order of 1,600 for a relative error of 2.5%.

Although it was assumed that the ADC was fast enough to avoid count-rate saturation and that the samples were free from impurities, pile-up rejection and peak overlapping, which both affect the accuracy of the least-squares fit at the tails of the Gaussians, were seen to induce an error in the fitting of the peaks. Indeed, the computer was expecting perfect Gaussian distributions and linear background.

With the statistical error, reduced by repeating each measurements three times, the final error on a typical integrated radiation may be approximated by 2.0% of its area.

PREPARATION OF STANDARDS AND CALIBRATION

1- The $Ga_xIn_{1-x}As_ySb_{1-y}$ system

This system represents a stoichiometric alloy of group III and group V elements from the periodic table: there are as many Gallium-Indium atoms as of Arsenic-Antimony. The x indicates the

relative abundance of the element Ga with respect to In; the general corresponding graphical representation being shown in FIG. 1-B, where the four corners are the compounds GaAs, GaSb, InAs, InSb and the sides, the ternary alloys $InAs_ySb_{1-y}$, $Ga_xIn_{1-x}Sb$, etc... In this diagram, point A will be represented by $Ga_{.20}In_{.80}As_{.39}Sb_{.61}$ and point B by $Ga_{.7}In_{.3}As_{.3}Sb_{.7}$ or $(GaSb)_{.7}(InAs)_{.3}$, since it happens to fall on the diagonal.

The x also gives the probability of a Gallium atom being present in a group III atom location of a regular lattice, zinc-blende structure here[8]. Hence if y is also the probability of an As atom being located at a group V atom location, the probability of having a Ga atom neighbouring an As atom will be xy. Similarly for an In atom to be adjacent to an Sb atom, it will be (1-x)(1-y), i.e. the product of their respective probabilities. From this we see that a general quaternary alloy $Ga_xIn_{1-x}As_ySb_{1-y}$ can be built up from the compounds GaAs, InAs, InSb and GaSb in the relative proportions of xy, (1-x)y, (1-x)(1-y) and x(1-y) per cent molar respectively.

The reason why the compounds were used instead of the elements and why this particular preparation method was employed will be given in the next two chapters.

2- Preparation of standards

The ideal standard would be in every way identical with the sample, but with the quantities of each constituent known. Matrix

effects and particle size effect (cf. below) would then be totally compensated. This paradoxical solution then implies the answer is known in advance of the analysis, for the composition of the unknown would be known. But it is possible to create an array of standards to map the region of interest and to interpolate accordingly. Preparing good homogeneous solid quaternary alloys to be used for calibration purposes is unfortunately almost impossible for most compositions. Annealing compounds gives inhomogeneous alloys while pure elements can hardly be mixed at all due to their very different metallurgical properties (e.g. melting point of Gallium, malleability of Indium,...). Moreover, solid standards with equivalent matrix enhancement as the unknown cannot be obtained by a quenching method.

Our solution was then to mix the binary compounds and to crush them into an intimate mixture which would approximate the properties of a solid sample. Particle size effect[2,6] and inter-compound enhancement is greatly reduced and becomes almost negligible with very fine powders (less than 10 microns diameter). High purity compounds were accurately weighted (to less than .2% error), crushed and mixed in a cylindrical aluminum piston, then powdered with a mortar and pestle. The resulting mixture was then deposited in a holder similar to those described above. The overall weight of a typical standard is 1.8 gr., and the loss occuring in the preparation being well approximated by 35 mg. This resultant 2.0% loss gives a negligible error compared to the count statistical

error and the fitting error, as seen above.

Each standard is then analysed three times by X-ray fluorescence to account for statistical fluctuations and inhomogeneity errors. Exposure times were twenty to forty minutes.

3- Scattering and matrix effects

A-Compton scattering: A typical noise and background spectrum is shown in FIG 5-A and 5-B. The constant low-count background may be attributed to scattered X-rays from the source-sample assembly and from the detector itself. The three wide peaks are Compton scattered X-rays through 180° of the Te characteristic radiation emitted by the source (TABLE 1-B).

B- Matrix effects: Matrix absorption and matrix enhancement refer to two effects whereby other constituents in the sample can alter the X-ray emission from a particular element. The direct consequence of this is that the intensity of an element's radiation is not only proportional to its concentration but also on the neighbouring elements. Methods of overcoming these effects have been extensively studied and reviewed in the recent literature, cf. Rhodes[2] for a comprehensive discussion of techniques used. The nature of the materials in the matrix, their concentration and the size of the particles are three problems which are almost impossible to overcome with a rigorous theoretical approach to a multi-element determination, because this would involve the product of many exponentials and require the knowledge of all the individual absorption coefficients relative to

all the different incident energies. Expressions have been derived, however, for a multi-elemental quantitative analysis using many approximations, together with the use of standards, neglecting all secondary and higher-order emission and absorption due to matrix effects.

C-Enhancement by the matrix: The most common situation, and this is particularly evident in our samples, occurs when an element is not only excited by the primary radiation, i.e. the source, but also by the characteristic X-rays of the other neighbouring constituents. The resultant intensity of an element is then the product of a complicated combination of absorption-enhancement interaction with the matrix. Let us consider a particular atom, say Arsenic, and its corresponding matrix of Gallium, Indium and Antimony atoms. The atomic process involved in fluorescence is then:

1-Excitation of the sample by the radioisotope with the corresponding emission of characteristic X-rays.

2-Absorption of the As X-rays by Gallium (matrix absorption) and absorption of the Indium and Antimony X-rays by As (matrix enhancement). The reverse process cannot occur since an element can receive energy only from an element which has higher X-ray energies; this may be expressed in terms of absorption coefficients.

3-X-rays produced by In as a direct consequence of the absorption of Sb X-rays are in turn absorbed by Arsenic,

whose radiation is then attenuated by Gallium, etc... (Higher order excitation).

Consequently, one may appreciate the difficulty in deriving an analytical expression accounting for the individual intensities of the four elements. For this quaternary alloy, a comparison method was then developed, together with the use of standards.

CALCULATION OF PEAK RATIOS AND CONCENTRATION OF THE UNKNOWNS

The output of all the samples was analysed by computer in order to obtain an accurate measure of the integrated peak intensities and their subsequent ratios: $\frac{Ga}{In}$, $\frac{Ga}{Sb}$, $\frac{As}{In}$, $\frac{Sb}{In}$, $\frac{Sb}{As}$ and $\frac{Ga}{As}$ all the symbols representing the intensities of the elements designed, i.e. Ga represents the integrated intensity of the Gallium peak: the area of the Gaussian distribution minus the background. These ratios are average values resulting from three analyses on X-ray fluorescence.

A particular intensity ratio will vary according to two parameters, say x and y, which we have chosen as the Gallium and Arsenic concentration (FIG. 1-B). FIG. 6 emphasizes

the fact, that for a given x, the ratio becomes a function of y; it also clearly demonstrates that, although the ratio $\frac{Ga}{Sb}$ is not very accurate in determining compositions for small y, it becomes useful for high values of y because of the large variation of the curve in that region of the graph: exponential on semi-logarithmic paper!

In FIG 7, matrix absorption and enhancement can account for the departure from a straight line of the ratio $\frac{Ga}{In}$, both being always in the same relative abundance (Ga=.9, In=.1, i.e. x=.9). Only matrix effects can then explain the dependance of the ratio with y. Finally, FIG 8 shows the whole family of curves for the ratio $\frac{Ga}{As}$.

FIG 9 and 10 give a general outlook of the final calibration. From these data and more detailed graphs of the form drawn 6, 7 and 8, it is now possible to determine within a per cent or two the composition of an unknown sample whose peak ratios have been obtained. This accuracy implies that one uses graphs where the particular ratio shows a large variation with composition. The average error on a ratio is approximately 4.0%, i.e. the sum of the error contribution from the two intensities involved and estimated above as 2.0%.

QUATERNARY ALLOYS OF III-V SEMICONDUCTORS

Miscibility of III-V semiconductors in the form of quaternary systems was first discussed in 1965 by Müller and Richards[8] for the systems $Ga_xIn_{1-x}As_yP_{1-y}$, $Ga_xIn_{1-x}P_ySb_{1-y}$, and $Ga_xIn_{1-x}As_ySb_{1-y}$

all of which crystallize in the zinc-blende structure. Flash evaporation was their method of compound preparation, the films of the desired composition being vapor deposited. Although complete solid solution occurred in the first system and a very small region of the phosphide-antimonide system, limited to two sides of the quaternary diagram, it was found that the $Ga_xIn_{1-x}As_ySb_{1-y}$ alloys had a miscibility gap completely enclosed by an area of solid solution. These authors account for this gap by taking into consideration the atomic radius mismatch of the individual constituents, a 17% mismatch being a good approximation for the critical value, in good agreement with their results.

More recently, William Coderre[10] prepared a few ingots of this $Ga_xIn_{1-x}As_ySb_{1-y}$ alloy by step-freezing GaAs and InSb. Assuming alloy formation along this direct tie line, i.e. the $(GaAs)_x(InSb)_{1-x}$ diagonal (TABLE 2-B), and Vegard's law for calculating the composition from the lattice parameter, he obtained alloys limited to the region $x>.85$, $x<.15$. This hypothesis that the resulting alloys will crystallize on the line corresponding to the initial constituents proportions cannot, however, be assumed in full confidence, and as will be seen, this hypothesis is in no way valid.

PREPARATION OF INGOTS AND SAMPLES

It was initially thought that homogeneous samples could be obtained from the melting and quenching of small amounts of the materials, but it was soon found out, from the analysis of X-ray Debye-Scherrer films taken at different points of the sample,

that such quaternary alloys had segregated, over the whole samples, into two phases. Ingot step-freezing was then performed. All the ingots were prepared from carefully weighted amounts of high purity compounds. The concern for getting accurately stoichiometric compounds, required for determination of composition by the XRF comparison method described above, and the relative simplicity of handling compounds rather than elements, e.g. Arsenic and Gallium, were two reasons for using III-V compounds instead of the elements Ga, As, In and Sb. The materials were placed in a quartz ampoule which was then evacuated and sealed. The furnace used for the step-freezing had a high temperature gradient which was obtained by a water-cooled baffle neighbouring a melting zone. The ampoule was first left in the high temperature zone, $1030\,^{\circ}C < T < 1090\,^{\circ}C$, for a few days in order to melt the materials completely and to allow them to diffuse, then a Meccano worm and gear assembly was used to pull the ampoule at a 1.5 centimeter per day constant speed. This velocity appeared to us as the fastest available gear speed capable of producing homogeneous ingots. Slices were then cut using a spark-cutter and etched with a 1:10 Bromine Methanol solution. The sharpness of the lines on Debye-Scherrer photographies was a good indication of the homogeneity of the samples.

ANALYSIS OF INGOTS

Data on the ingots is given in FIG 11,12,13,14,15. In all the quaternary diagrams displayed, the cross indicated the initial

constituent composition, i.e. $Ga_{.26}In_{.74}As_{.26}Sb_{.74}$ for Ingot A in FIG 11. These diagrams also show the variation of composition along the ingot, as determined by XRF, while the bottom graph represents the lattice parameter change with distance along the ingot, for example running from 5.698 Å near the GaAs end to 6.479 Å for InSb in FIG 11. The dotted line on this diagram is a rough estimate of the weak second phase present in these samples together with the strong phase, represented by the solid line. A consequence of this second phase is the error introduced in the top figure by the composition determination, which is meaningful, with respect to the phase diagram, only when one phase is concerned. This weak second phase, which corresponds to the composition of the single phase samples on the other side of the gap, is then an indication of a too rapid speed of growth. This ingot was step-freezed too fast. From lattice parameter results (cf. graph below), from the knowledge of compositions on both sides of the gap, by XRF, and from a qualitative determination of their relative abundance, it may be shown that the true single phase composition of these samples should had fallen on the curve indicated by the circles. Still in FIG 11, the dashed and the dotted lines are tie lines on the peritectic plane of the phase diagram and indicate the spread of the gap. The dashed line on the lattice constant graph corresponds to this peritectic region.

FIG 12, 13, 14, 15 give similar results for alloys of different

starting points. In FIG 14, this point was not well defined and is represented by a distorted cross , and the dashed lines in both diagrams represent the expected continuation of these curves when a qualitative composition determination of slices cut at the end tail of the ingots is made. Similarly for FIG 15.

PHASE DIAGRAM AND LATTICE PARAMETER

One of the prime objects of this work was to study the behaviour of the lattice constant for this quaternary alloy, in such a way to enable someone to determine the composition of a sample, knowing its lattice parameter and other characteristics (phase diagram, starting composition of ingots...). This would have eliminated the requirement of powdering the solid samples for XRF analysis. Unfortunately, only a very limited number of homogeneous single-phase materials were obtained, which is explained by a much larger miscibility gap than expected. Indeed, Müller and Richards[8] had predicted a gap extending from GaAs 85%, InSb 15% to InSb 85%, GaAs 15% on the $(GaAs)_x(InSb)_{1-x}$ diagonal, and from InAs 30%, GaSb 70% to GaSb 20%, InAs 80% on the $(GaSb)_x(InAs)_{1-x}$ diagonal. The circle line approximates this gap in FIG 16-B while the dotted line represents our estimate of the size of the gap, using the tie lines on the peritectic plane obtained from this work. Of course, these lines are drawn between the last single phase materials which crystallized at both ends of the composition gap.

Point A and B in FIG 16-B were obtained from studies of the

$GaAs_xSb_{1-x}$ system by M. Gratton (private communication). They correspond to the observed boundaries of the peritectic gap on the phase diagram and were found to be approximately $GaAs_{.35}Sb_{.65}$ and$GaAs_{.85}Sb_{.15}$.

The difficulty of analysing the samples at the edges of the gap may be estimated by the very rapid composition and lattice parameter change over a small space interval (FIG 11, 12, 13). Consequently, the ends of the tie lines on the peritectic surface are not well defined, but it still remains obvious, from all the data collected, that the gap is much larger than was predicted by Müller and Richards. Unfortunately, the absence of any experimental results near the InAs corner prohibits any extrapolation of the gap area in that region.

Other useful information on the phase diagram of this quaternary alloy is the direction of the tie lines connecting points on the liquidus surface. They relate the molten constituents composition with the first crystallized solid samples of the ingot. Five of these tie lines are shown in FIG 17. The length of these lines is consistent with the large peritectic gap expected and the large horizontal spread between liquidus and solidus lines which usually occurs in these III-V compounds, i.e. $Ga_xIn_{1-x}As$, $InAs_xSb_{1-x}$, $GaAs_xSb_{1-x}$... This preliminary investigation on the $Ga_xIn_{1-x}As_ySb_{1-y}$ phase diagram will serve as a guide to future research and analysis on the preparation of these alloys.

The lattice constant was measured accurately on Debye-Scherrer X-ray diffraction films by locating the position of the highest angle diffracted lines. The data was fed into a computer which gave out the lattice parameter, calculated from the Bragg reflection law using correction factors. Since a sample with a uniform composition will only yield one set of bright, sharp lines, the thickness of the lines gives information on the homogeneity of the samples, as previously mentioned On some occasions, the presence of additional lines, which are observed mainly near the low order lines, may indicate the presence of any other phase. The dotted line in the lattice constant diagram of FIG 11 represents such a second phase coexisting with the majority phase, indicated by a solid line.

The lattice constant results are displayed in FIG 16-A. As mentioned above, only a very limited number of homogeneous single phase quaternary alloys were obtained, and, consequently, lattice parameter results cover only three small corners of the $Ga_xIn_{1-x}As_ySb_{1-y}$ system. As expected, the curve segments are approximately along the GaSb-InAs diagonal direction since these two compounds have almost similar lattice constants (6.0959 Å and 6.0585 Å respectively), and these curves are of increasing value, from the low GaAs lattice parameter value (5.6535 Å) to InSb (6.4789 Å).

CONCLUSION

The study of the $Ga_xIn_{1-x}As_ySb_{1-y}$ system cannot be dissociated from a preparation analysis, which in turn, is associated with composition determination and phase diagram research. This was the purpose of this work, together with the investigation of the lattice constant variation. However, it was found that very few single phase alloys could be produced, because of a large peritectic gap in the phase diagram. The problem of composition determination of the samples gave rise to the elaboration of a relatively new comparison method by X-Ray Fluorescence with the use of powdered standards. Hence information was obtained on the phase diagram and on the lattice constant variation.

Much work remains to be done in the preparation of new ingots and samples before the complete phase diagram of this alloy system is known. This preliminary study will serve as a guide towards such a result.

REFERENCES

1 Recent Advances in X-Ray Detector Technology by D.W. Aitken
Transaction on Nuclear Science, IEEE, NS-15, no. 3, 1968, p. 10

2 Radio-Isotope X-Ray Spectroscopy by J.R. Rhodes
The Analyst, vol. 91, no. 1088, 1966

3 The Future of Silicon X-Ray Detectors by D.W. Aitken and E. Woo
Kevex Corp., Calif., Special Technical Publication 485, 1971

4 Determination of Rare Earth Elements in Rocks... by H. Kunzendorf and H.A. Wollenburg.
Nuclear Instruments and Methods, 87, 1970, p. 197-203

5 Detection Limit for Silver for ... by P.G. Burkhalter
International Journal of Applied Radiation and Isotopes
vol. 20, 1969, p.353-362

6 Effect of Particle Size on Backscattered X-Ray. Corrections Methods in On-stream X-Ray Fluorescence Analysis
by K.G. Carr-Brion. The Analyst, vol. 91, 1966, p. 289

7 Radioisotope X-Ray Techniques For On-stream Analysis of Slurries
by W.K. Ellis et al. International Jour. of Applied Radiation and Isotopes, vol. 20, p. 691-701, 1969

8 Miscibility of III-V Semiconductors Studied by Flash Evaporation
by E.K. Müller and J.L. Richards. Jour. of Applied Physics, vol. 35, number 1, pp. 1233-1241, 1964

9 Nuclear Physics, An Introduction by W.E. Burcham
Longmans Green and Co Ltd (London), p. 197

10 Ph.D. Thesis by William M. Coderre
University of Ottawa, 1969, p.26 and 46

11 Elements of X-Ray Diffraction by B.D. Cullity
Addison-Wesley Publication Co. Inc., 1967, p. 6

TABLE 1

1-A I^{125} source: radiations emitted

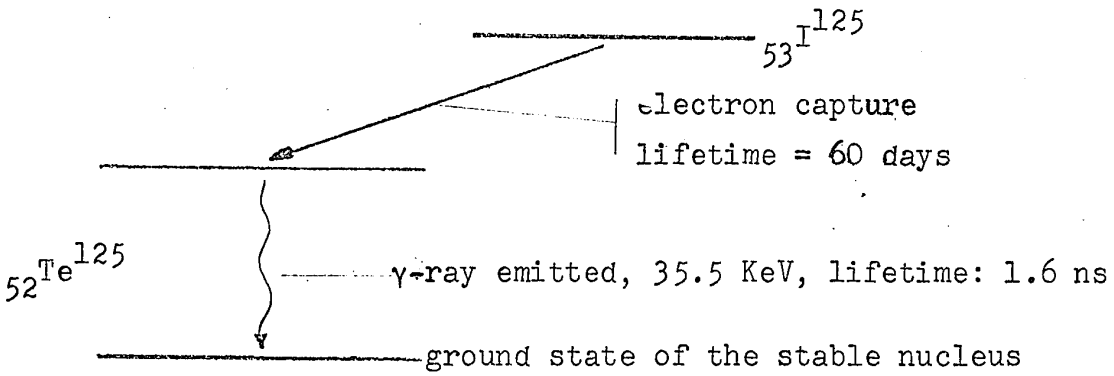

$$_{53}I^{125} + e^{-} \rightarrow {}_{52}Te^{125} + \gamma$$

The Te characteristic X-rays are also emitted due to internal conversion and to excitation of the Te atoms by the 35.5 KeV radiation. The vacancy in one of the innermost shells, created by electron capture, causes a characteristic radiation transition to occur.

Useful radiations emitted from the source and their relative intensities are then:

27.4 KeV Te K_α X-rays	80%
31.0 KeV Te K_β X-rays	14.5%
35.5 KeV γ-ray	5.1%

1-B Approximate energy of Compton backscattered radiation:

Compton scattering[9]: $$E' = \frac{E_o}{1 + \frac{E_o}{mc^2}(1-\cos\theta)}$$

where E' = scattered radiation (in KeV)

E_o = incident radiation (in KeV)

mc^2 = rest mass of an electron = 511 KeV

$\theta = 180^\circ$ for backscattering

Hence:

Incident radiation energy E_o (in KeV)	Backscattered radiation energy E' (in KeV) $E' = \frac{E_o}{1+0.0039 \cdot E_o}$
gamma ray 35.5	31.17
Te K_{α_1} 27.47	24.81
K_{α_2} 27.27	24.65
K_{β_1} 30.99	27.65
K_{β_2} 31.70	28.21

1-C X-ray emission energies: (in KeV)

atomic number	element	K_{α_1}	K_{α_2}	K_{β_1}	K_{β_2}
31	Gallium	9.25	9.22	10.26	10.36
33	Arsenic	10.54	10.50	11.72	11.86
49	Indium	24.21	24.00	27.27	27.86
51	Antimony	26.35	26.11	29.72	30.38

FIGURE 1

1-A Gallium resolution vs count rate:

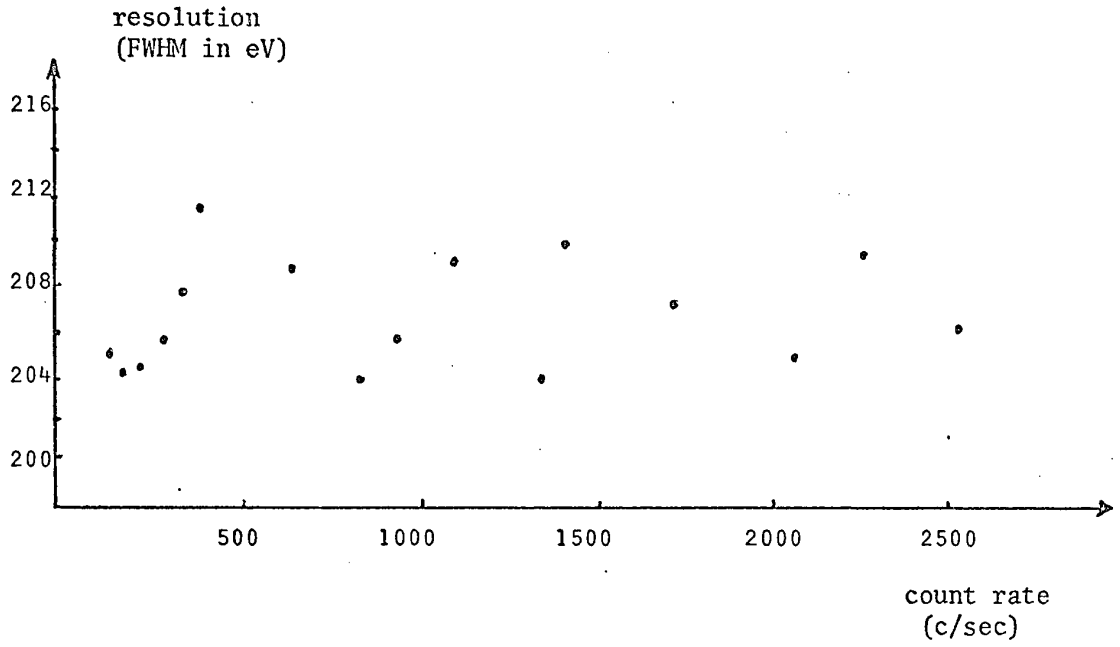

1-B The $Ga_xIn_{1-x}As_ySb_{1-y}$ system:

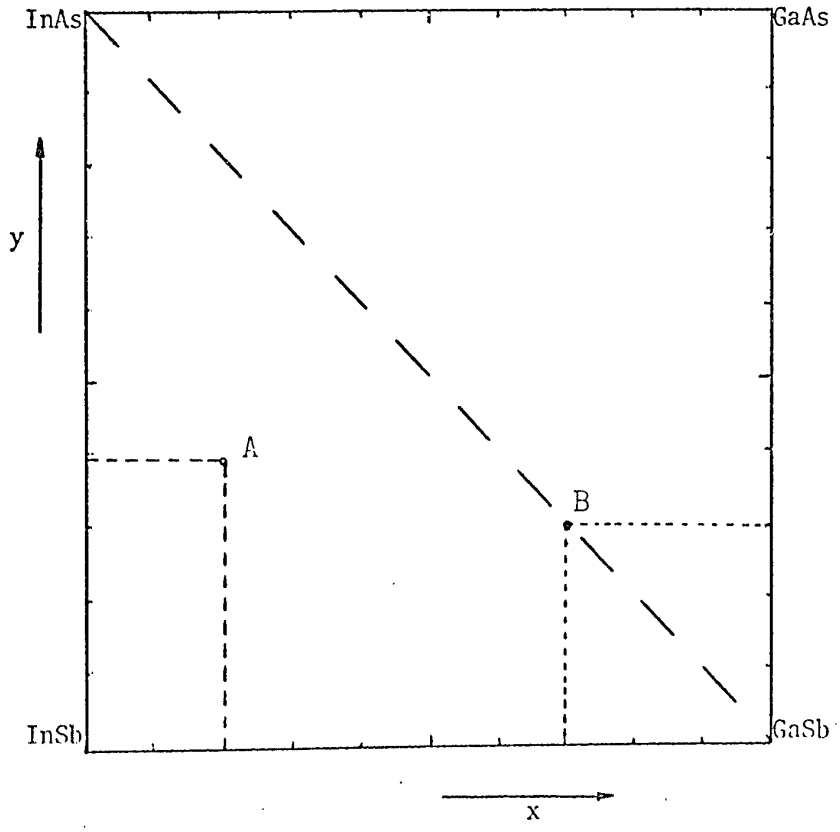

FIGURE 1-C

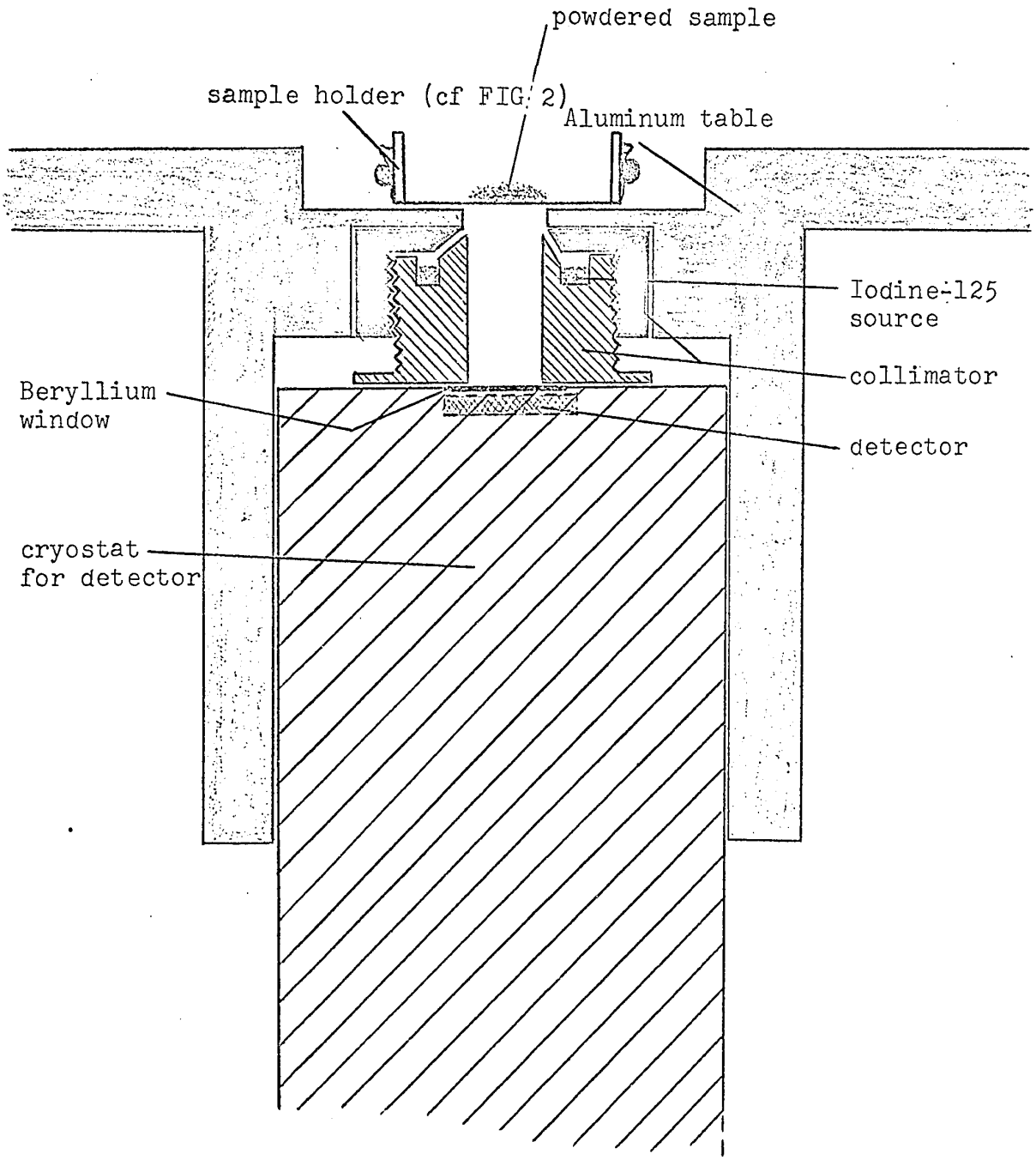
powdered sample
sample holder (cf FIG. 2)
Aluminum table
Iodine-125 source
collimator
Beryllium window
detector
cryostat for detector

FIGURE 2

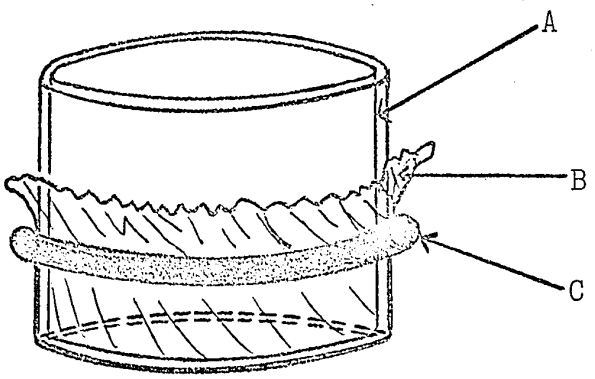

SAMPLE HOLDER: A polyethelene "saran" wrap (C) is stretched at the bottom of a one inch piece of acylic tubing (A). An O-ring (C) secures the thighness of the very thin wrap on which powders are placed, at the centre. Radiation absorption by the polyethelene is negligible.

FIGURE 3 : Electronics for XRF

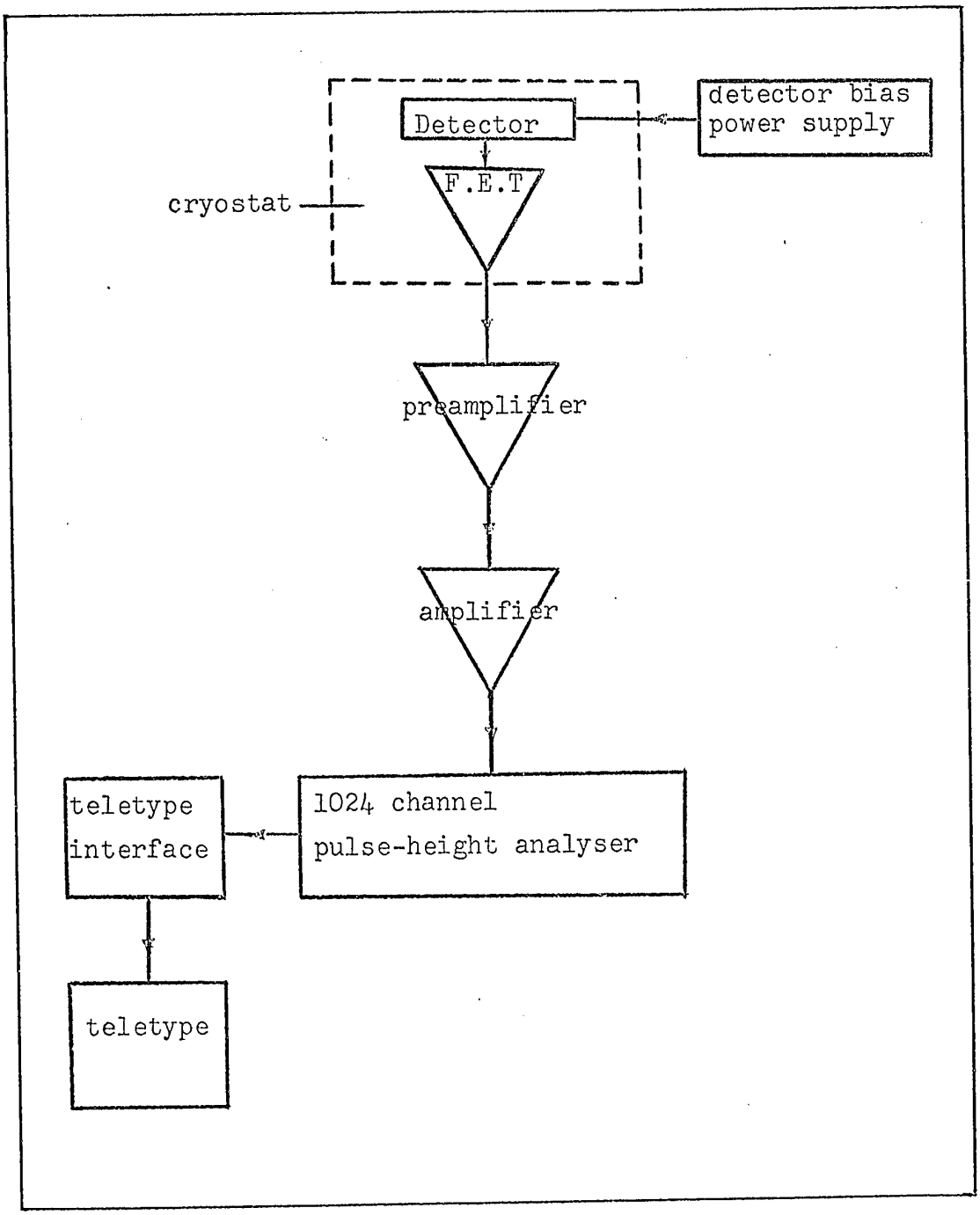

FIGURE 4: Typical spectrum from a quaternary alloy.

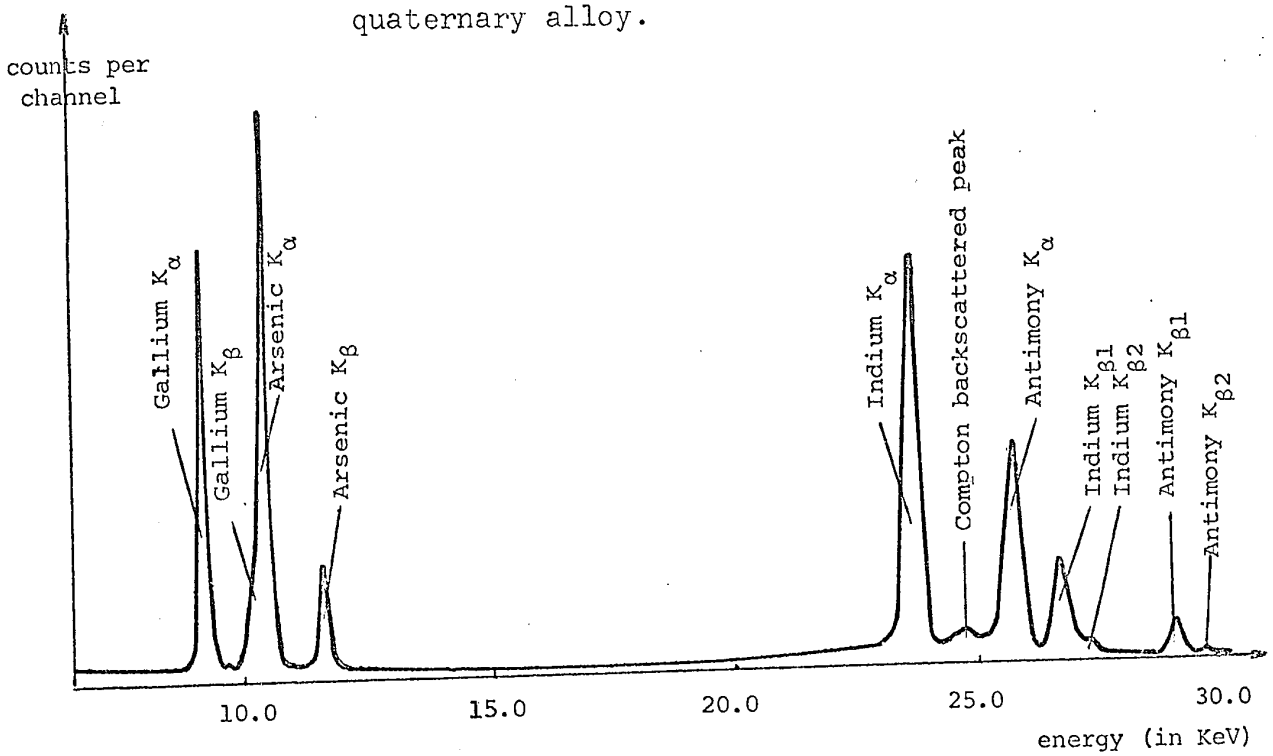

4-A Linear scale

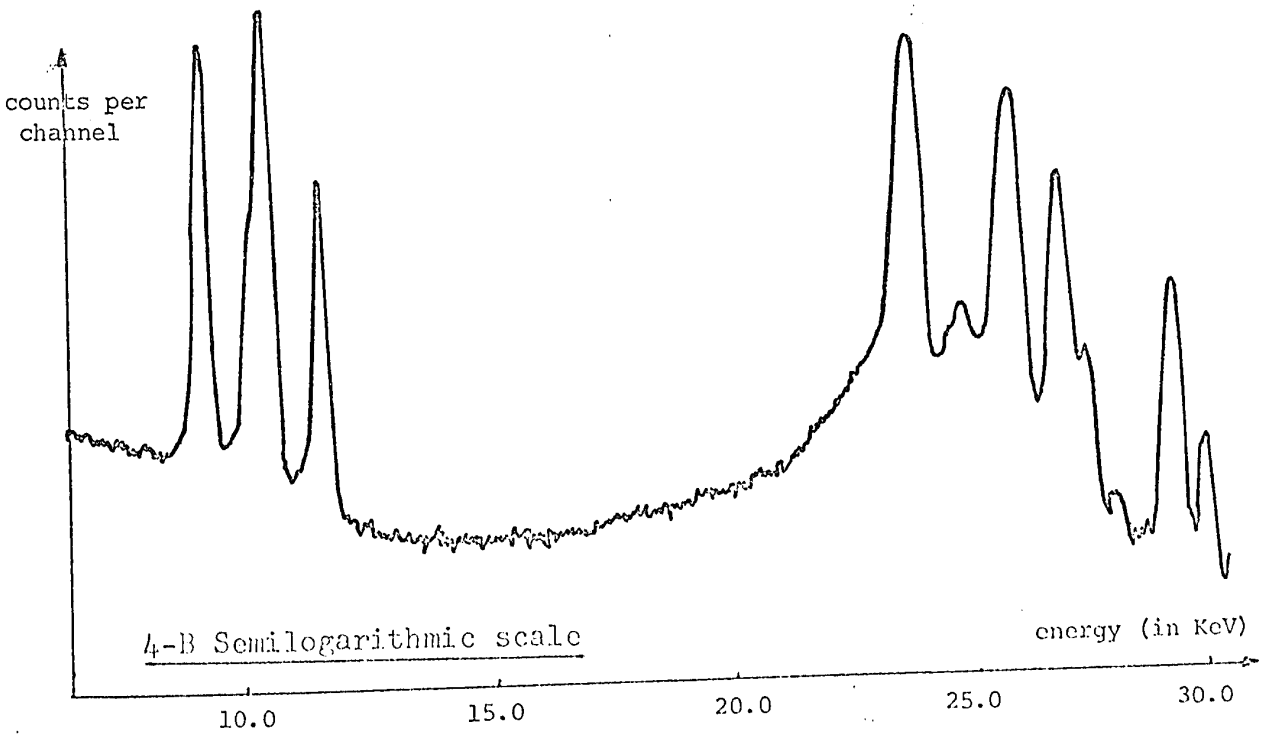

4-B Semilogarithmic scale

FIGURE 5: Typical backscattered spectrum
Energy of peaks is given
in TABLE 1-B.

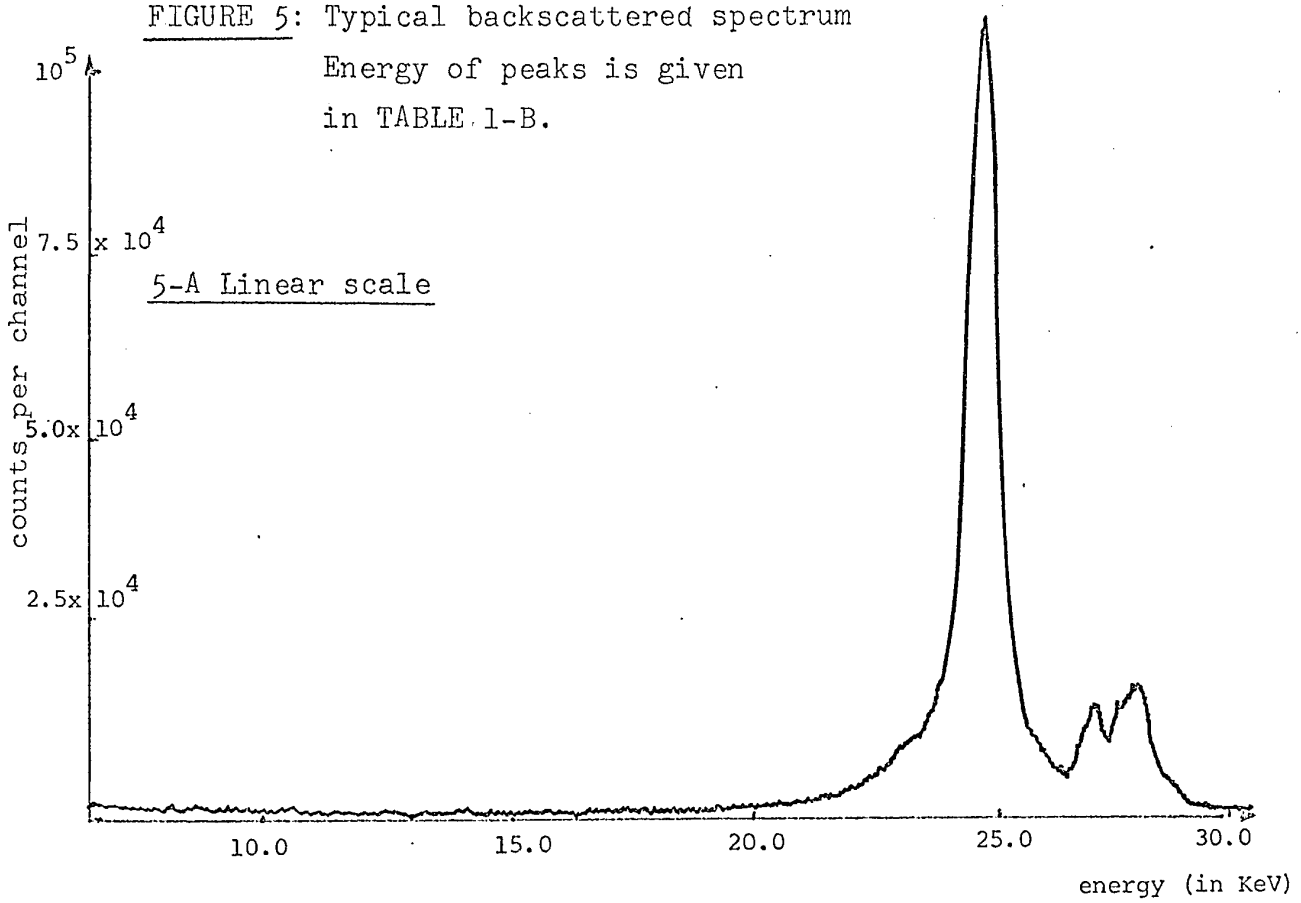

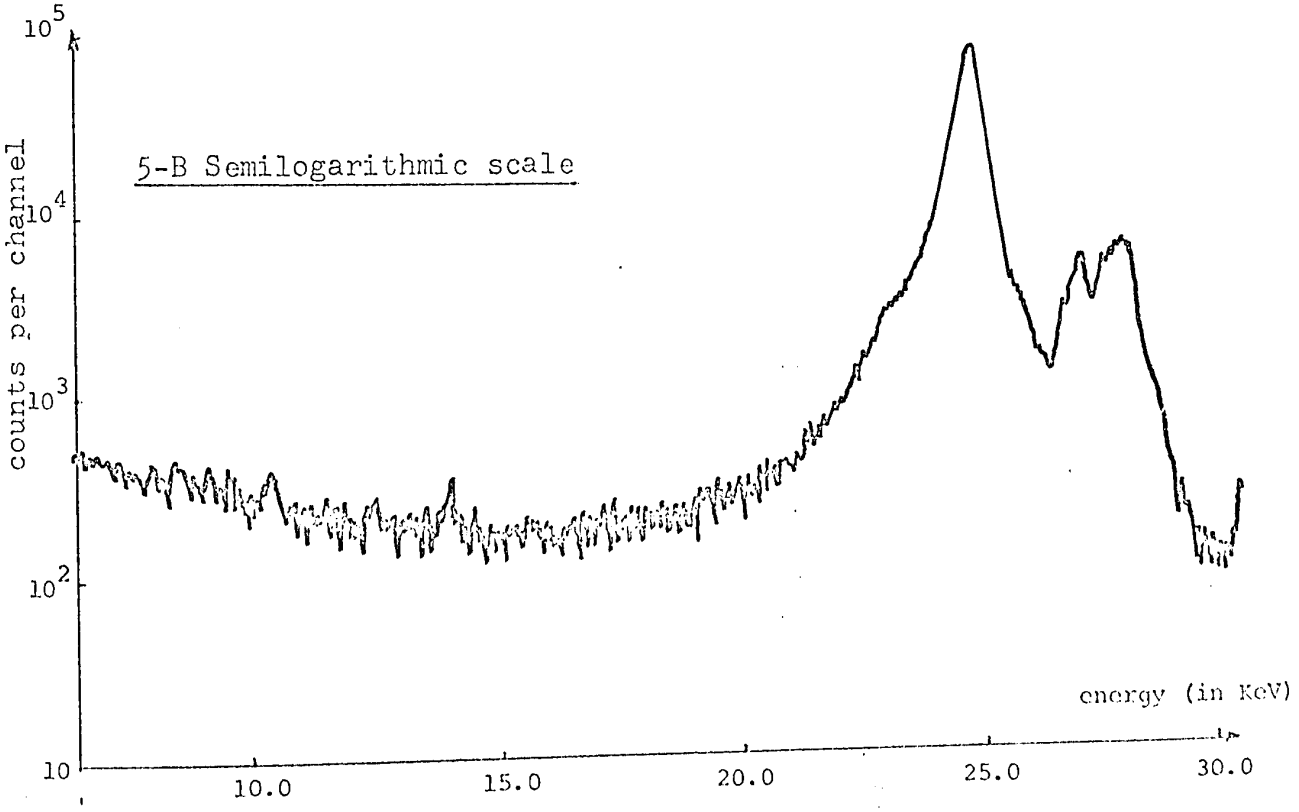

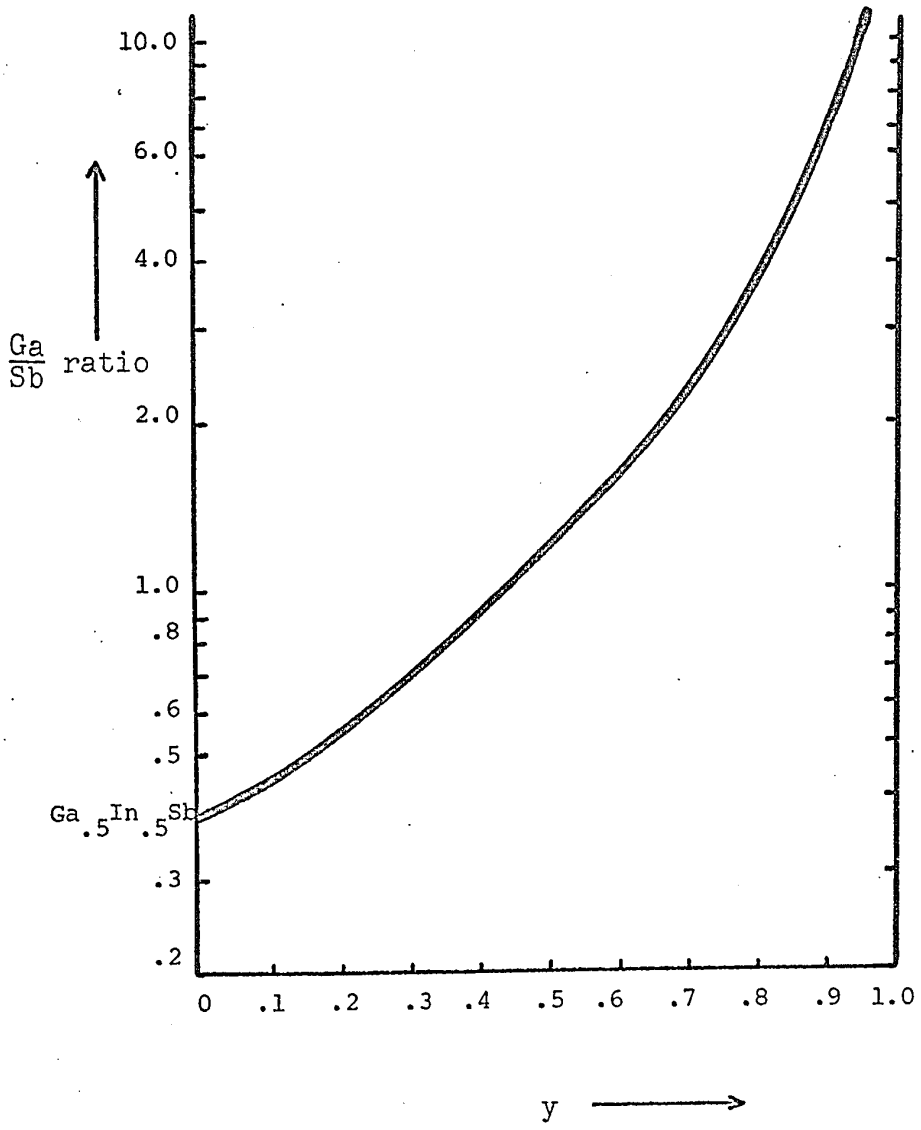

FIGURE 6: $\frac{Ga}{Sb}$ ratio as a function of the Arsenic concentrarion y, in $Ga_{.5}In_{.5}As_ySb_{1-y}$. The thickness of the curve is a measure of the uncertainty. This curve was determined from seven measurements.

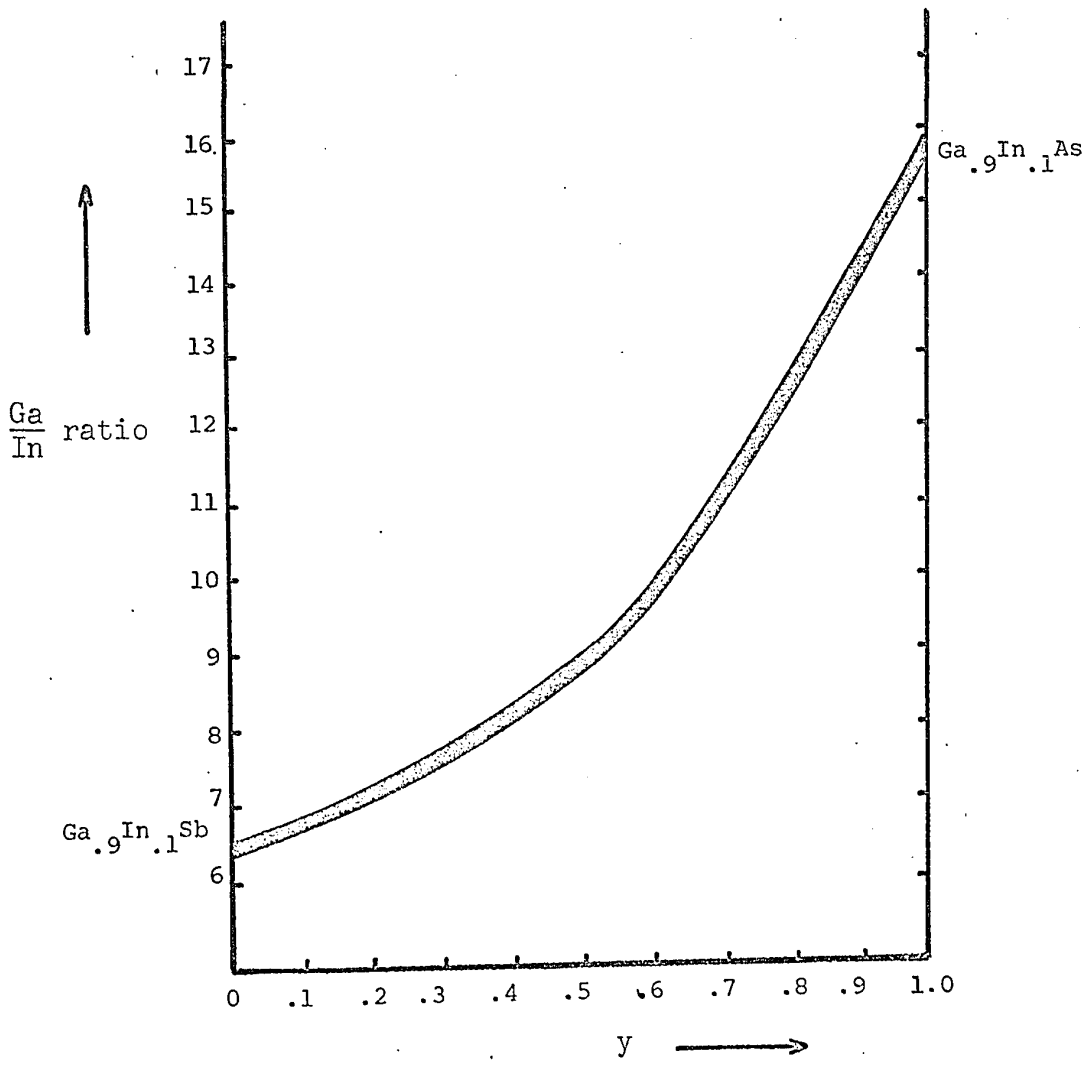

FIGURE 7: $\frac{Ga}{In}$ ratio as a function of the Arsenic concentration y, for x=.9 . The thickness of the curve is a measure of the uncertainty. This curve was drawn from seven points.

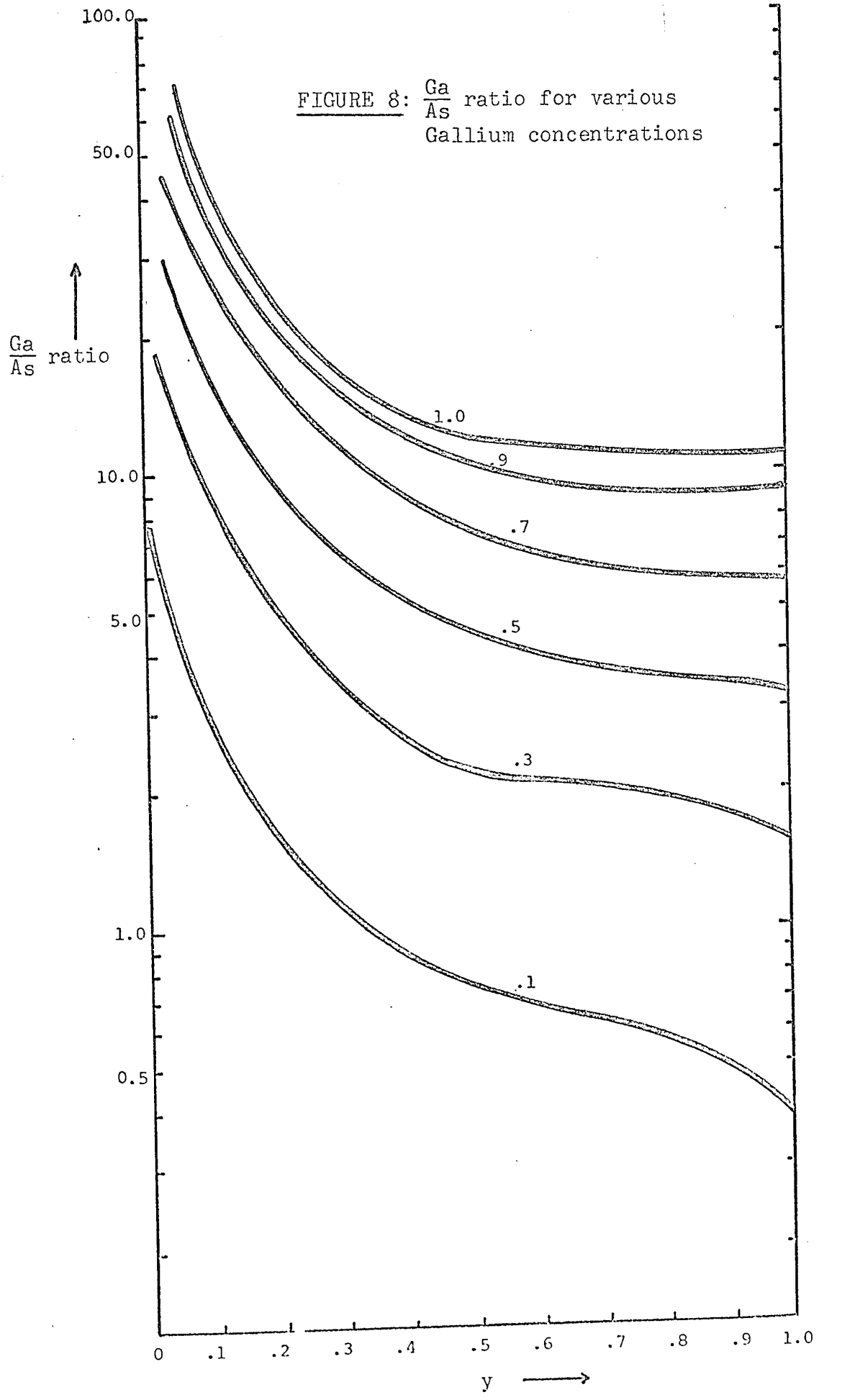

FIGURE 8: $\frac{Ga}{As}$ ratio for various Gallium concentrations

FIGURE 9

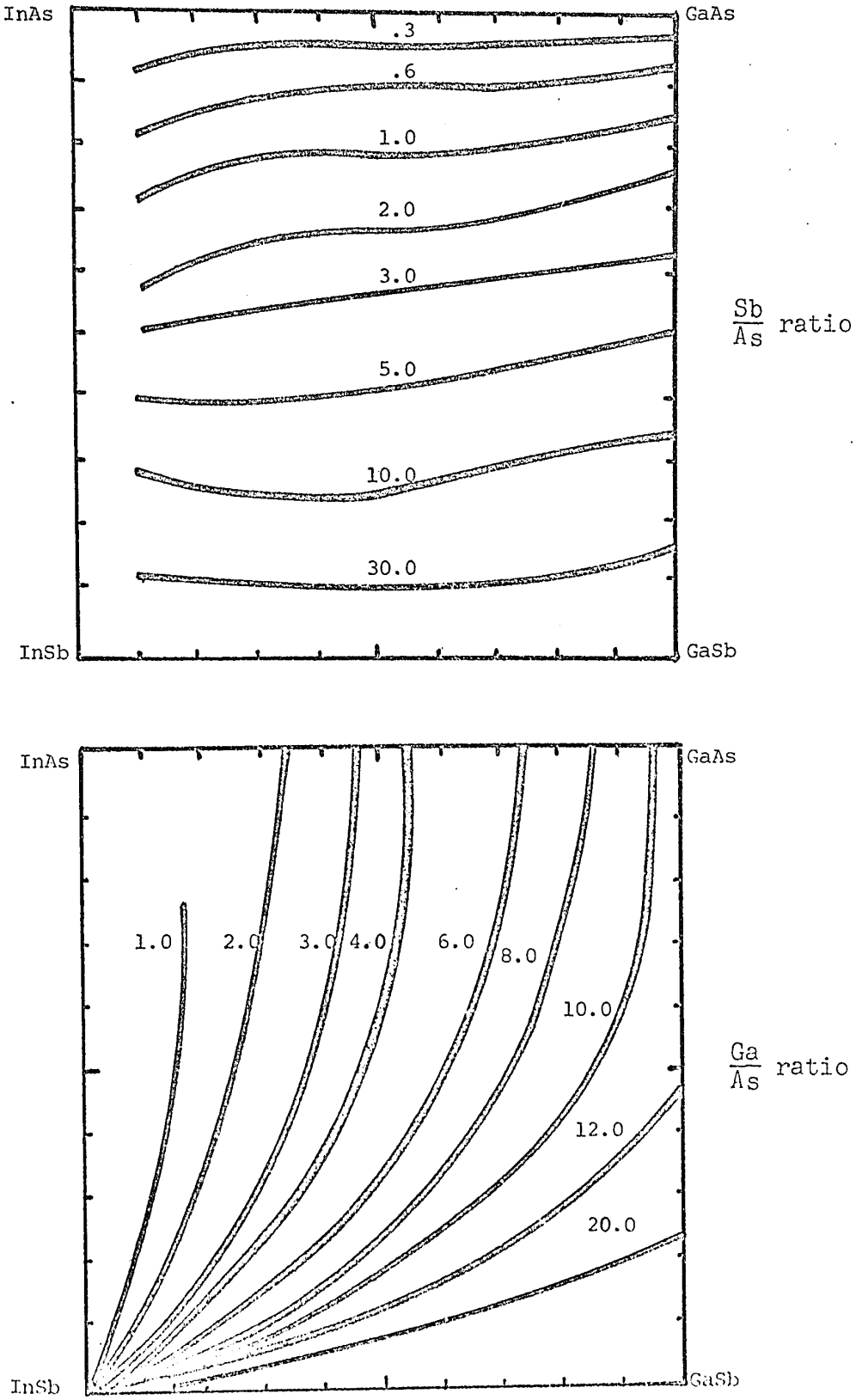
InAs
GaAs
.3
.6
1.0
2.0
3.0
5.0
10.0
30.0
InSb
GaSb
Sb/As ratio
InAs
GaAs
1.0
2.0
3.0
4.0
6.0
8.0
10.0
12.0
20.0
InSb
GaSb
Ga/As ratio

FIGURE 10

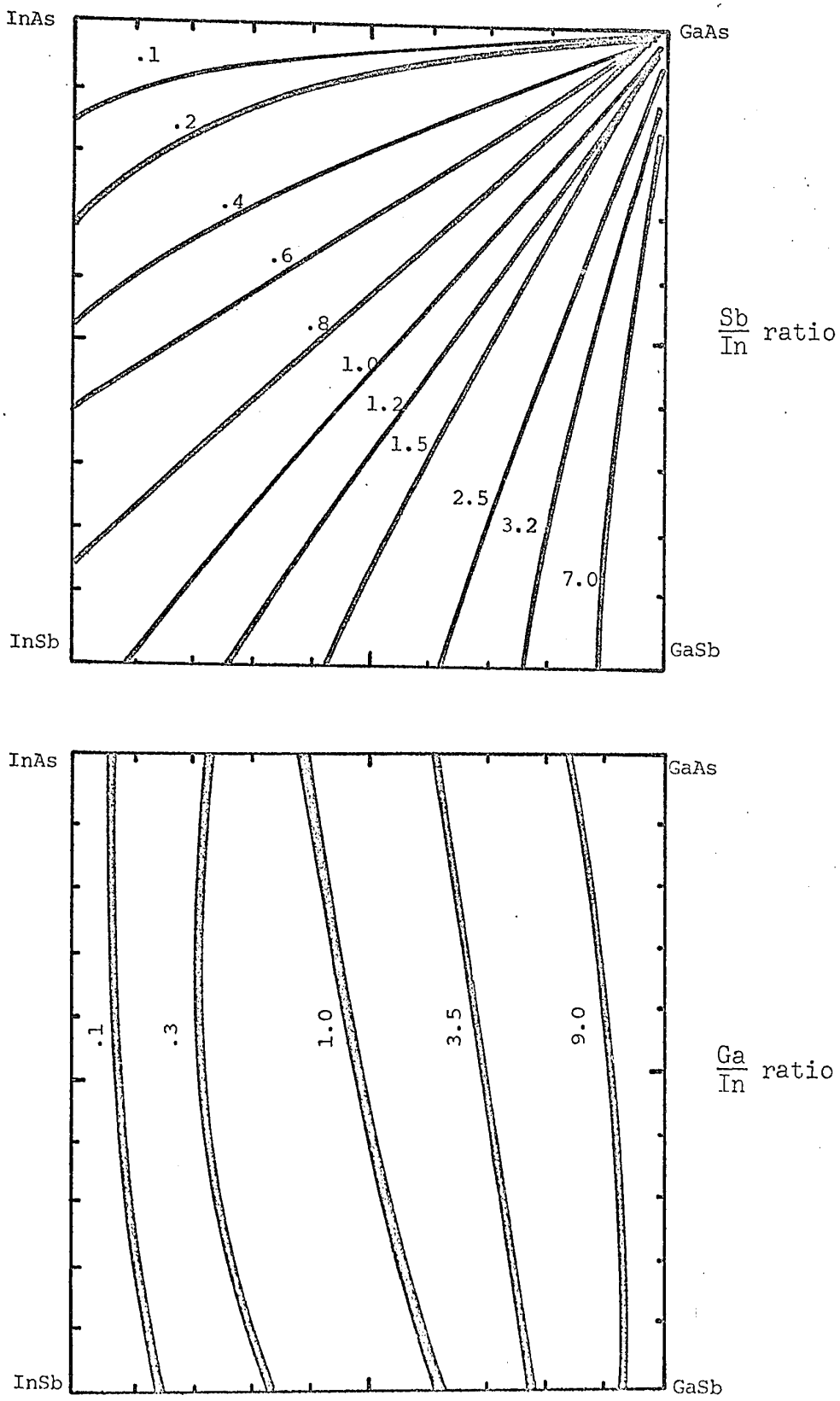
InAs
GaAs
.1
.2
.4
.6
.8
1.0
1.2
1.5
2.5
3.2
7.0
InSb
GaSb
Sb/In ratio
InAs
GaAs
.1
.3
1.0
3.5
9.0
InSb
GaSb
Ga/In ratio

FIGURE 11: Data on ingot A

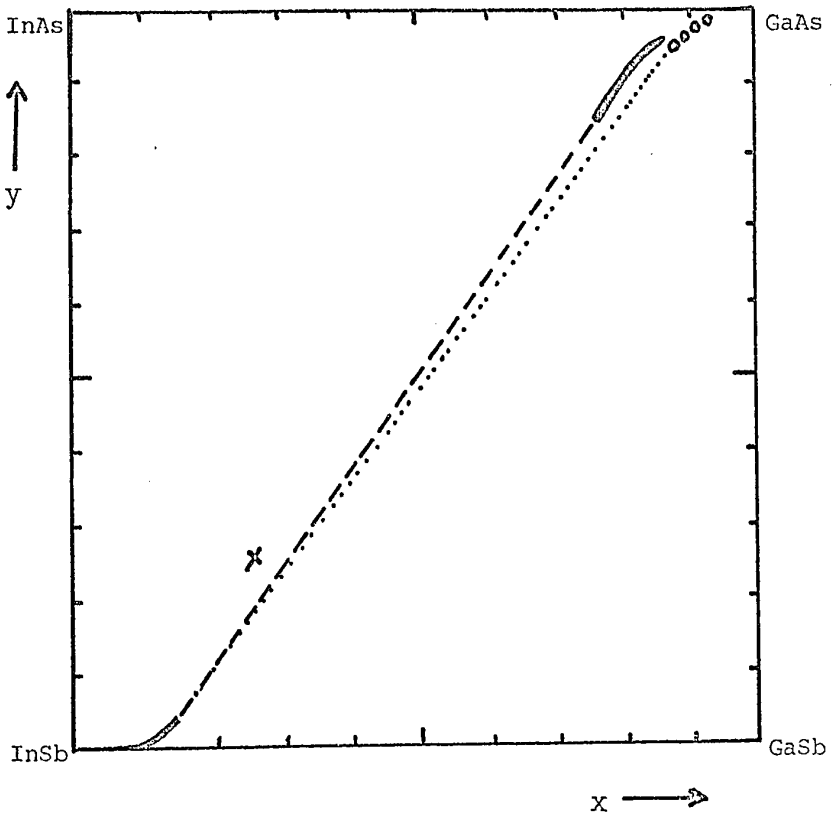

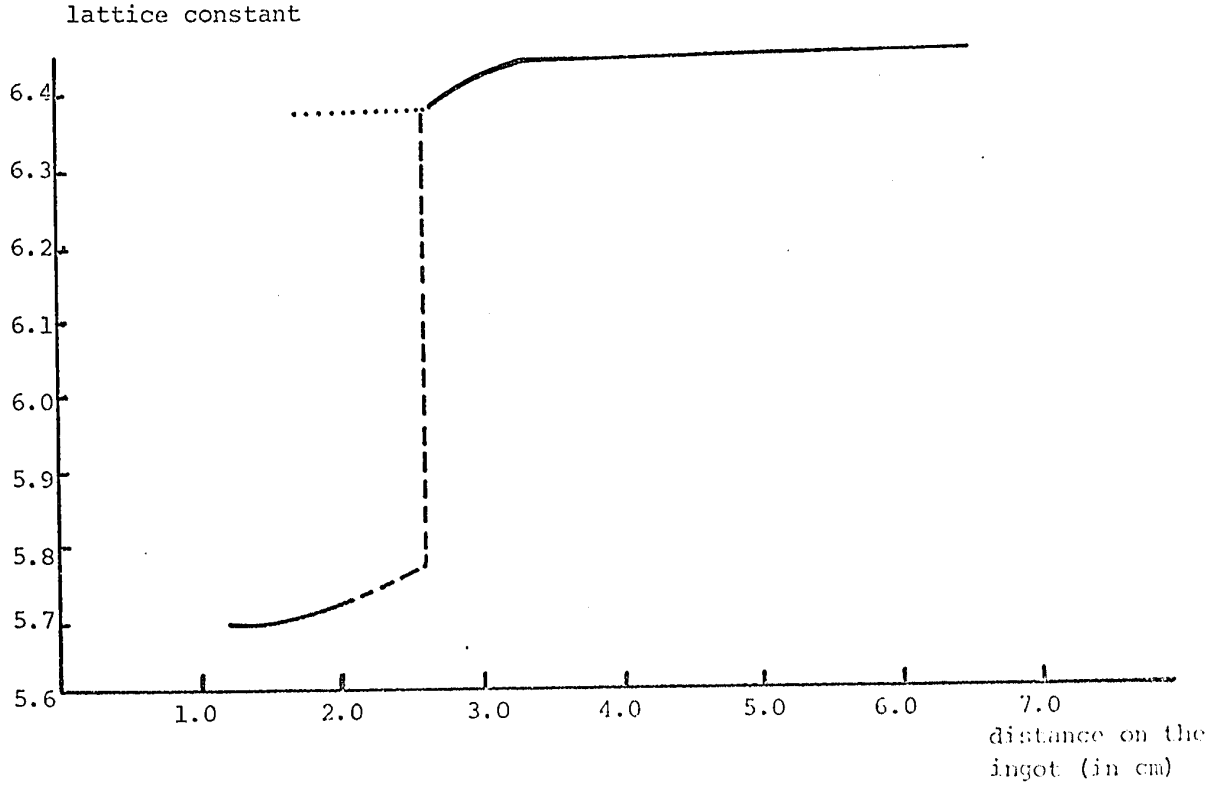

FIGURE 12: Data on ingot B

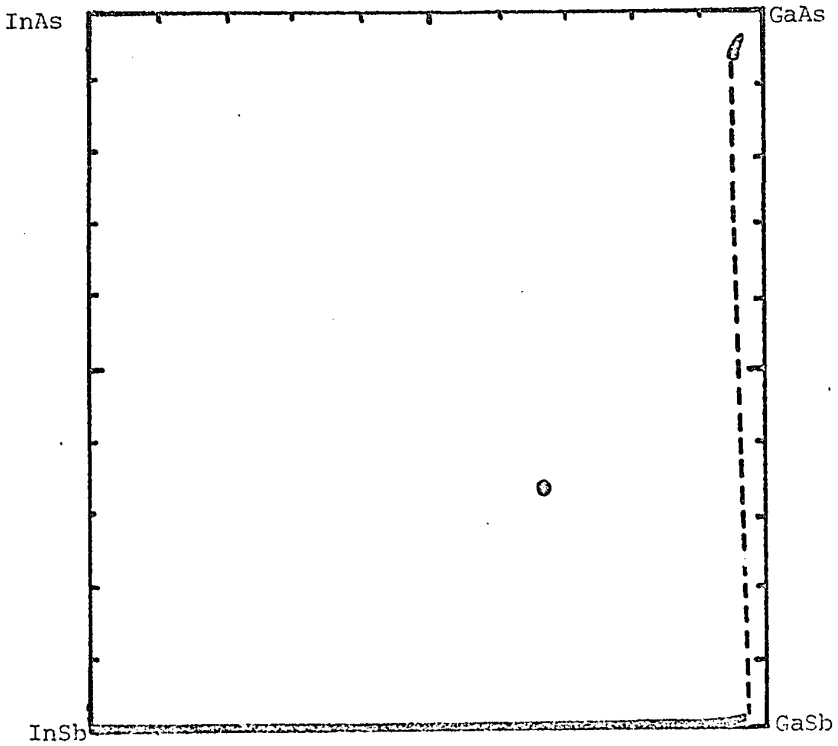

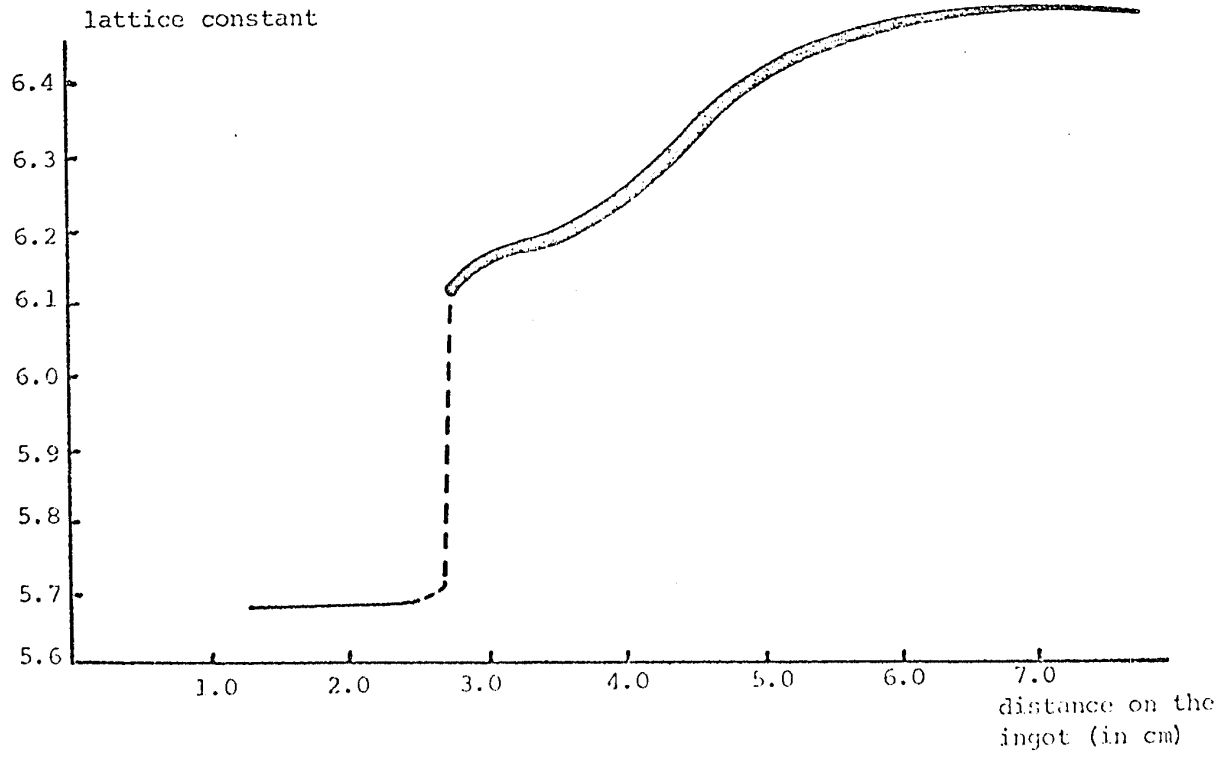

FIGURE 13: Data on ingot C

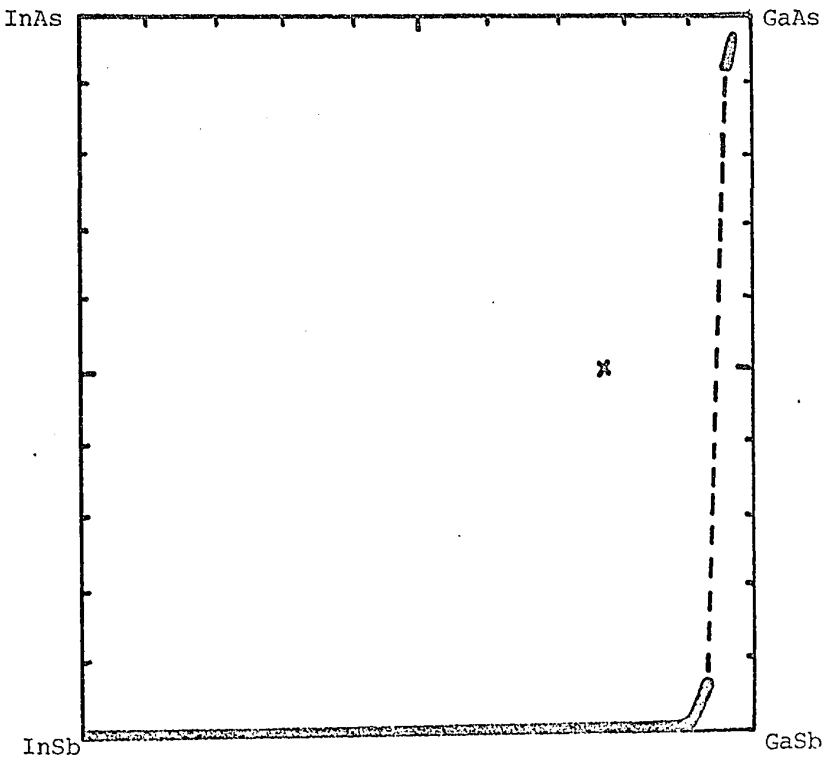

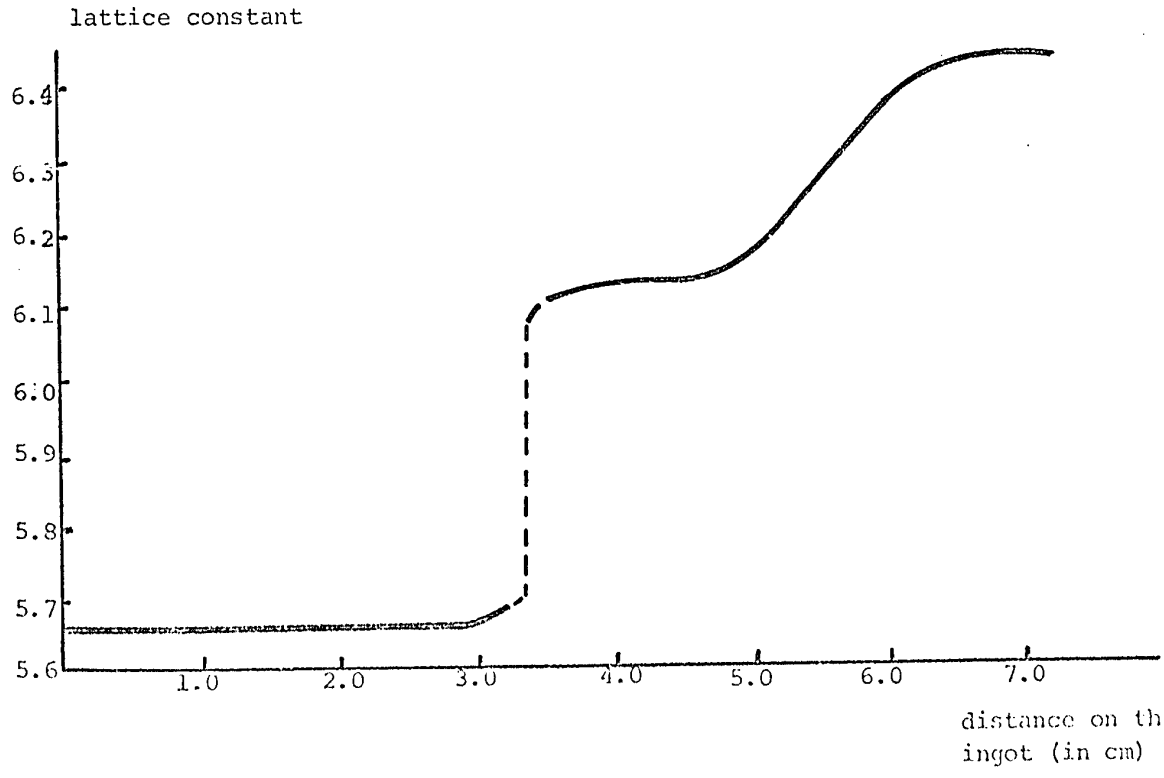

FIGURE 14: Data on ingot D

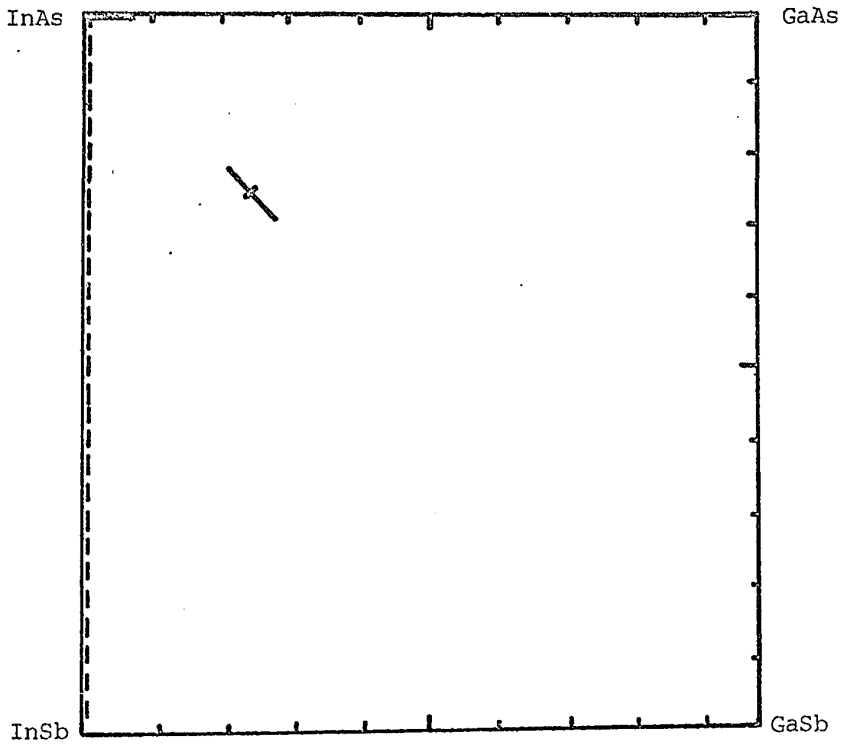

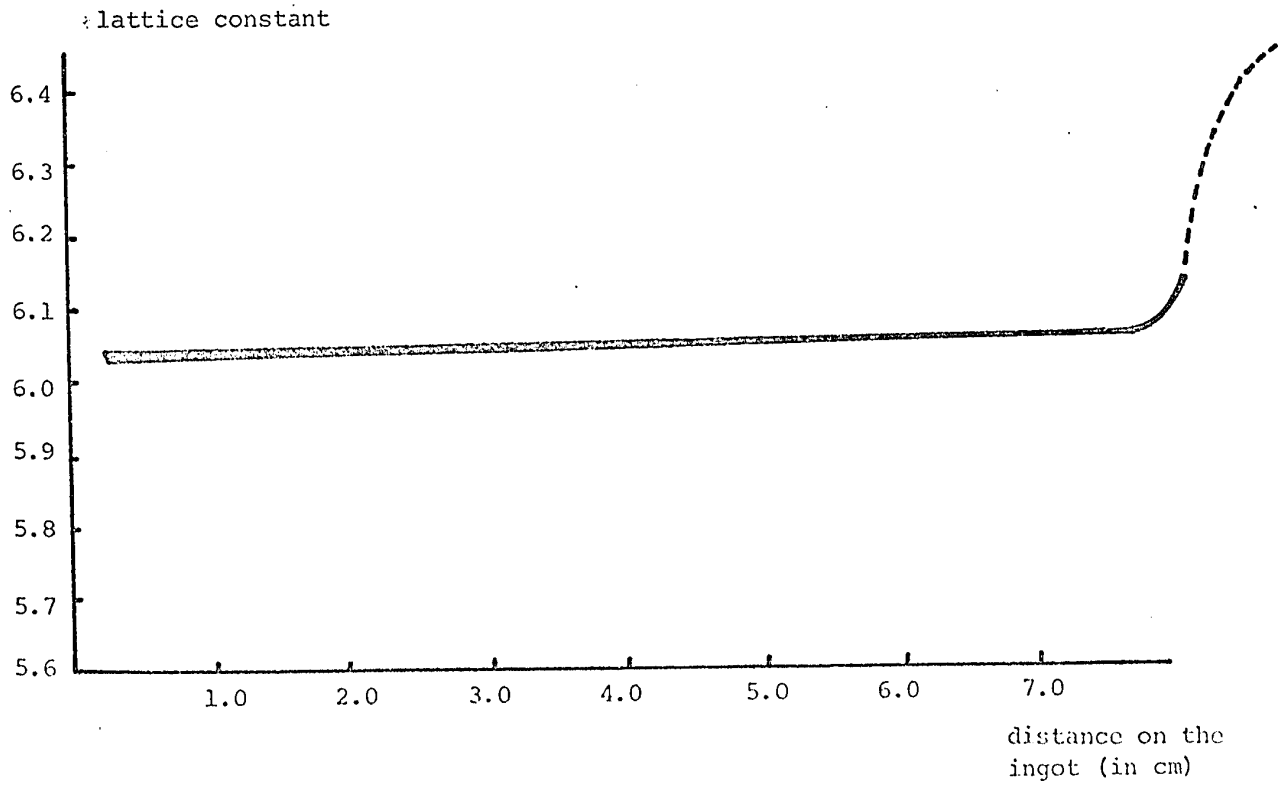

FIGURE 15: Data on ingot E

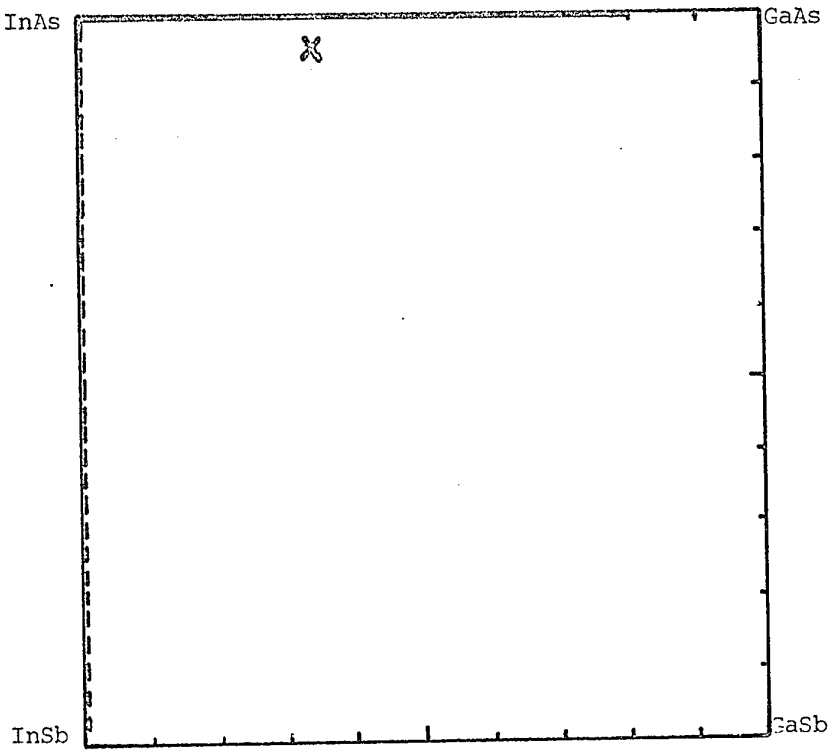

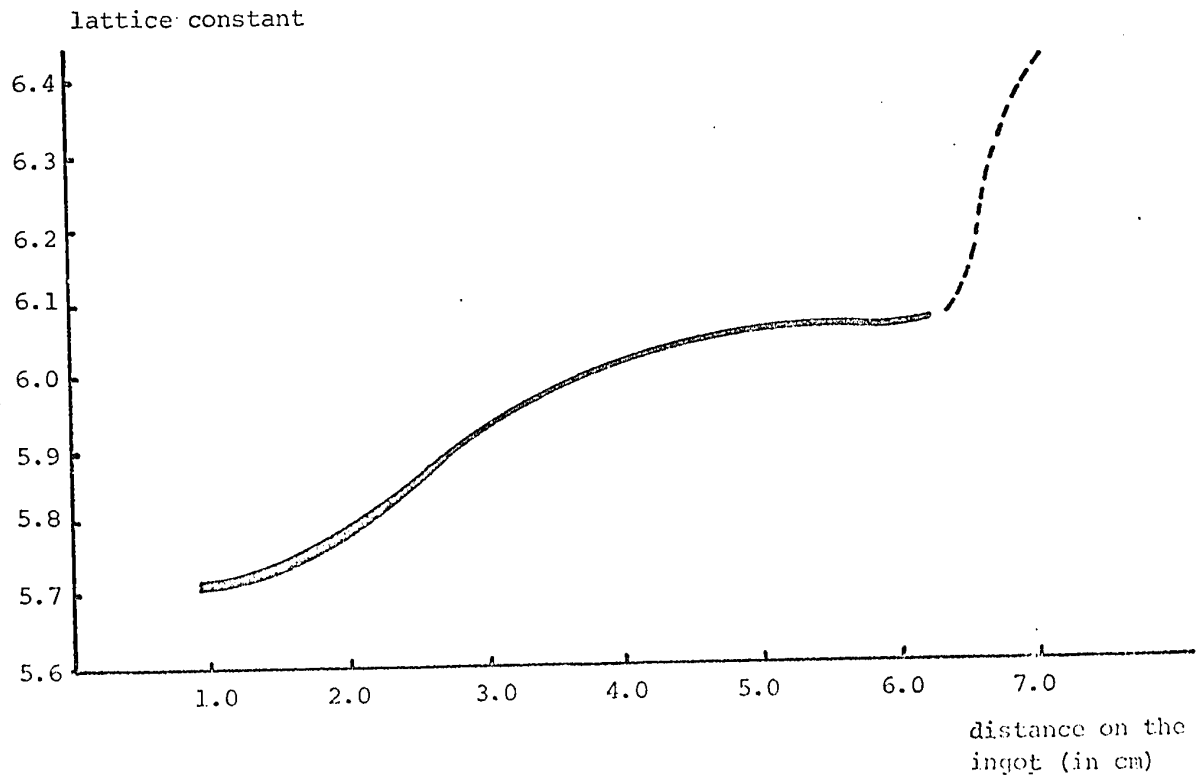

FIGURE 16

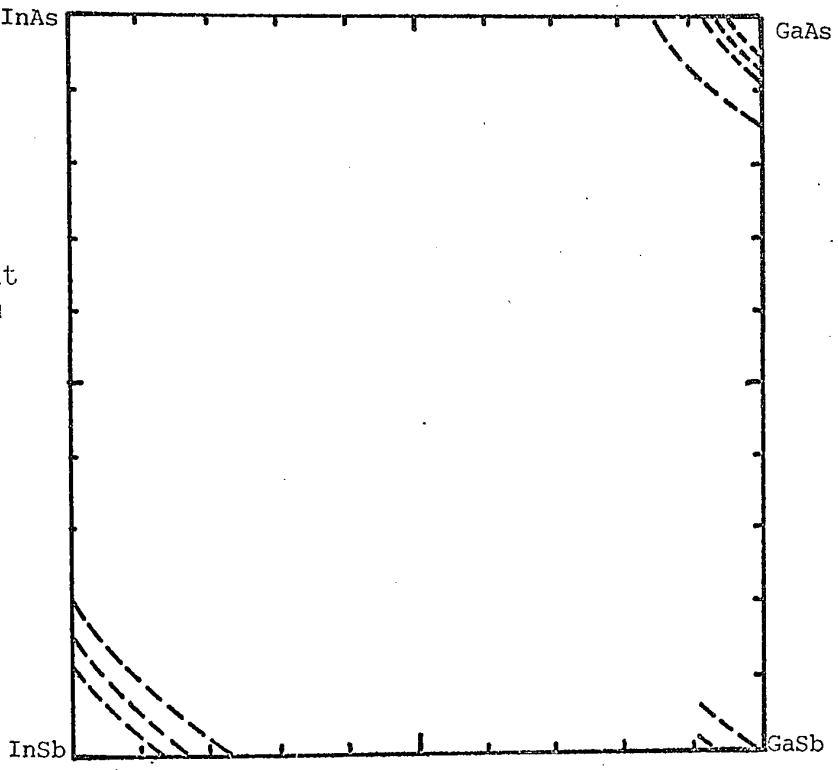

16-A lattice constant diagram

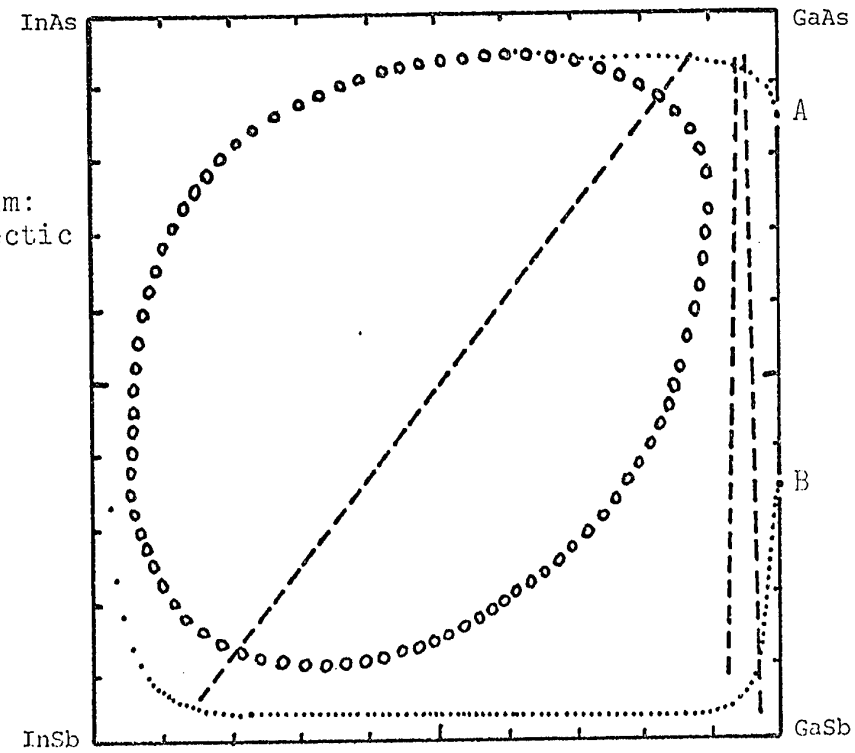

16-B phase diagram: peritectic gap

FIGURE 17: Phase diagram tie lines